

Asymmetric protonation of glutamate residues drives a preferred transport pathway in EmrE

Jianping Li⁺, Ampon Sae Her⁺, Nathaniel J. Traaseth^{*}

Department of Chemistry, New York University, New York, NY 10003

⁺ These authors contributed equally to this work

* Corresponding author: traaseth@nyu.edu

Abstract

EmrE is an *Escherichia coli* multidrug efflux pump and member of the small multidrug resistance (SMR) family that transports drugs as a homodimer by harnessing energy from the proton motive force. SMR family transporters contain a conserved glutamate residue in transmembrane 1 (Glu14 in EmrE) that is required for binding protons and drugs. Yet the mechanism underlying proton-coupled transport by the two glutamate residues in the dimer remains unresolved. Here, we used NMR spectroscopy to determine acid dissociation constants (pK_a) for wild-type EmrE and heterodimers containing one or two Glu14 residues in the dimer. For wild-type EmrE, we measured chemical shifts of the carboxyl side chain of Glu14 using solid-state NMR in lipid bilayers and obtained unambiguous evidence on the existence of asymmetric protonation states. Subsequent measurements of pK_a values for heterodimers with a single Glu14 residue showed no significant differences from heterodimers with two Glu14 residues, supporting a model where the two Glu14 residues have independent pK_a values and are not electrostatically coupled. These insights support a transport pathway with well-defined protonation states in each monomer of the dimer, including a preferred cytoplasmic-facing state where Glu14 is deprotonated in monomer A and protonated in monomer B under pH conditions in the cytoplasm of *E. coli*. Our findings also lead to a model, *hop-free exchange*, which proposes how exchangers with conformation-dependent pK_a values reduce proton leakage. This model is relevant to the SMR family and transporters comprised of inverted repeat domains.

Significance Statement

EmrE is a proton-coupled efflux pump that confers multidrug resistance to *Escherichia coli*. Here, we probed the electrostatic environment surrounding each essential Glu14 residue in the EmrE dimer by determining monomer specific pK_a values using NMR spectroscopy. We discovered that acid/base chemistry at one of the two Glu14 residues in the homodimer potentiates a global conformational change within EmrE. Our findings revealed that asymmetric protonation states of EmrE leads to a preferred pathway of substrate transport. These insights led to a model to explain how EmrE accomplishes proton-coupled transport without leaking protons. Since the overall structure of EmrE resembles those of other transporters containing inverted repeat domains, our findings have application to other secondary active transporters.

Introduction

Antibiotic resistance arises from multiple molecular mechanisms, including enzymatic breakdown of drugs, mutations of target proteins, reduced drug influx, and the activation of efflux pumps (1). The efflux mechanism by membrane protein transporters is one of the broadest resistance mechanisms that requires active transport to reduce the internal drug concentration. Four out of five drug efflux families are secondary active transporters and share the following features: (i) broad binding specificity to toxic compounds including antibiotics, antiseptics, and cationic dyes, (ii) undergo conformational exchange to catalyze the substrate transport across the membrane, and (iii) contain essential anionic residues needed for binding protons and/or substrates.

E. coli EmrE from the SMR family has served as a model of drug transport since it contains the minimal required complexity (110 residues) and shares each of the features found in other drug transporters. Namely, it forms an antiparallel homodimer that is required for drug efflux (2-6), it undergoes conformational exchange needed for drug transport (7, 8), and it contains a conserved anionic residue at Glu14 in each monomer of the dimer that is essential for antiport of protons (3, 5, 6, 9-11). While these studies provided insight into features of EmrE needed for drug efflux, key questions remain about the ion-coupled transport mechanism. Specifically, it is unclear whether the two Glu14 residues can exhibit differential protonation states in a lipid bilayer environment and whether deprotonation at one monomer influences the acid dissociation constant (pK_a) of the other monomer in the dimer (i.e., electrostatic coupling).

Here, we used NMR spectroscopy and pH titrations to quantify chemical shift perturbations of Glu14 and surrounding residues in a monomer specific manner within the EmrE dimer. These measurements allowed us to derive monomer specific changes for accurately

assessing the Glu14 protonation states within EmrE and determine that the two Glu14 residues in the dimer have independent pK_a values. Using our findings, we propose a transport model for EmrE with Glu14 protonation states specified for each monomer and discuss the implications of this model for minimizing proton leakage while achieving efficient proton-coupled drug efflux.

Results

Asymmetric Glu14 protonation in EmrE determined using solid-state NMR spectroscopy

We aimed to determine protonation states of Glu14 in EmrE using NMR spectroscopy by directly detecting the ^{13}C chemical shift of the carboxyl carbon since this observable strongly correlates with the protonation state (12). Uniformly $^{13}\text{C}/^{15}\text{N}$ labeled, wild-type EmrE was reconstituted into lipid bilayers comprised of diether lipids (*O*-14:0-*O*-PC) to ensure stability throughout NMR data collection at different pH values. Double-quantum single-quantum REDOR (DQSQ-REDOR) (13) magic-angle-spinning spectra were acquired on EmrE samples at pH values of 5.0, 8.0, and 10.0 (Figure 1a). The three anionic residues in EmrE (Glu14, Glu25, Asp84) were clearly resolved in the spectra at each pH value, with assignments confirmed using mutagenesis and $^{13}\text{C}/^{13}\text{C}$ correlation experiments (14) (Supplemental Figure 1). Of these residues, only Glu14 experienced a chemical shift perturbation from pH 5.0 to 10.0. The chemical shift at pH 5.0 was 176.0 ppm (Figure 1a, top panel), while its chemical shift at pH 10.0 was 180.8 ppm (Figure 1a, bottom panel). The protonated chemical shift of Glu14 was \sim 8 ppm upfield from the solvent accessible Glu25 residue within EmrE, which likely reflects the hydrophobic environment surrounding this side chain within the substrate binding pocket. However, the difference of 4.8 ppm between chemical shifts at pH values of 5.0 and 10.0 matches with the expected span between protonated and deprotonated side chains of glutamate

residues (12). Therefore, we conclude that Glu14 residues are predominantly proton-bound at pH 5.0 ($E_A^H-E_B^H$) and deprotonated at pH 10.0 ($E_A^-E_B^-$), where E_A and E_B correspond to each monomer of the EmrE crystal structure bound to tetraphenylphosphonium (15). Note that association of monomers in the crystal structure with NMR experiments is based on the agreement of helical tilt angles estimated from the structure and those determined using oriented sample solid-state NMR spectroscopy (16-19).

In contrast to NMR spectra at pH 5.0 or 10.0, we observed two peaks for Glu14 of EmrE in the DQSQ-REDOR spectrum at pH 8.0 that matched the chemical shifts of the protonated and deprotonated species (Figure 1a, middle panel). This result suggested the two Glu14 residues had asymmetric protonation states in the dimer. To test this hypothesis, we prepared heterodimer samples by mixing wild-type EmrE with the L51I mutant ($EmrE^{L51I}$) (19). Such samples result in a preferred conformational equilibrium where wild-type EmrE occupies monomer B position in the heterodimer and $EmrE^{L51I}$ occupies monomer A position (Supplemental Figure 2). DQSQ-REDOR spectra of $^{13}\text{C}/^{15}\text{N}$ labeled EmrE mixed with unlabeled $EmrE^{L51I}$ and the opposite isotopic labeling scheme were acquired at pH values of 5.0, 8.0, and 10.0 (Figure 1b and 1c). Unlike the two peaks observed for Glu14 in the wild-type spectrum at pH 8.0, each heterodimer sample displayed a single peak for Glu14 at pH 8.0. Namely, the carboxyl chemical shift for Glu14 of monomer B (EmrE) in the heterodimer appeared at 176.2 ppm, indicating a protonated state (Figure 1c, middle panel), while Glu14 of monomer A ($EmrE^{L51I}$) appeared at 180.8 ppm, indicating a deprotonated state (Figure 1b, middle panel). As a control, we observed Glu14 carboxyl chemical shifts at pH values of 5.0 and 10.0 for each heterodimer sample that were in agreement with those observed in the corresponding wild-type EmrE spectrum. From these data, we conclude EmrE contains Glu14 residues that are asymmetrically protonated in lipid bilayers,

where Glu14 in monomer A is more acidic ($5.0 < pK_a < 8.0$) than that of monomer B ($8.0 < pK_a < 10.0$).

pK_a values determined using solution NMR spectroscopy

To determine pK_a values in a monomer specific manner, we used solution NMR spectroscopy in DMPC/DHPC isotropic bicelles since it was more robust for collecting several datasets over a range of pH values. We employed our heterodimer technology involving EmrE and EmrE^{L51I} and performed pH titrations on samples where only one protein was isotopically enriched. $^1\text{H}/^{15}\text{N}$ TROSY spectra showed that the conformational equilibrium of the EmrE-EmrE^{L51I} heterodimer was maintained from pH 5.0 to 10.0 and at a temperature of 37 °C needed for collecting high-quality NMR spectra (Supplemental Figure 3; Supplemental Figure 4). The change in conformational equilibrium induced by the L51I mutation in the EmrE-EmrE^{L51I} heterodimer corresponds to a free energy of ~1.8 kcal/mol (19). Note that the heterodimer approach overcame the limitation of pH dependent conformational exchange previously observed in wild-type EmrE (8, 20), which complicates spectral analysis and does not afford monomer specific chemical shift perturbations (CSPs) to be quantified (8, 21).

CSPs in monomers A and B were quantified from $^1\text{H}/^{15}\text{N}$ TROSY spectra for several residues within the EmrE-EmrE^{L51I} heterodimer. Monomer A peaks displayed several large CSPs, including for residues Gly9_A and Gly17_A that are close in proximity to Glu14_A (Figure 2a, Supplemental Figure 4a). Monomer B peaks also displayed large CSPs for Gly9_B and Gly17_B that are near Glu14_B (Figure 2b, Supplemental Figure 4b). Notably, we observed a striking non-linear CSP for Gly17_B (Figure 2b), indicative of a multi-step process. This observation suggested that Gly17_B was sensitive to acid/base chemistry at both Glu14 residues in the dimer, consistent

with the asymmetric Glu14 protonation state observed in solid-state NMR experiments (Figure 1). We globally fit CSPs in proximity to Glu14 using a modified Henderson-Hasselbalch equation with two pK_a values (Equation 1), yielding values of 7.2 ± 0.1 and 8.4 ± 0.2 (Figure 2c and 2d). These solution NMR results support the conclusion that under a physiologically relevant temperature of 37 °C and cytoplasmic pH of 7.5, the preferred state of EmrE is bound to one proton in monomer B ($E_A^- \cdot E_B^H$). Our observations are in agreement with pK_a values reported by Morrison *et al.* (21) (7.0 ± 0.1 and 8.2 ± 0.3) and the ΔpK_a computed by Vermaas *et al.* (22) ($\Delta pK_a = 1.08$); however, our findings contrast with the pK_a values reported by Ovchinnikov *et al.* (8.80-9.32 and 10.45-11.38) (23).

Deprotonation of Glu14 in monomer A triggers a global conformational change

In pH titration experiments of the EmrE-EmrE^{L51I} heterodimer, most residues displayed CSPs that coincided with the more acidic pK_a value, suggesting Glu14_A deprotonation induced the more significant conformational change within the dimer. To test this hypothesis, we prepared a heterodimer with a single Glu14 residue in the dimer by mixing EmrE with the E14Q mutation of EmrE (EmrE^{E14Q}). Similar to other heterodimer samples, isotopically enriched EmrE or EmrE^{E14Q} was mixed with the partner protein at natural abundance and ¹H/¹⁵N TROSY spectra were acquired at several pH values (Figure 3a, b; Supplemental Figure 4c, d). For each pH value, isotopically enriched EmrE in the heterodimer displayed more intense monomer A signals, while isotopically enriched EmrE^{E14Q} displayed more intense monomer B signals. Using monomer A and B peak intensities, we estimated free energies of the conformational equilibria at ~3.5 kcal/mol for pH 9.5 and ~0.6 kcal/mol for pH 6.2 (see Materials and Methods). The larger free

energy difference at the basic pH value indicated a greater preference for the deprotonated Glu14 in the heterodimer to occupy the monomer A position.

Several residues in monomers A and B of the EmrE-EmrE^{E14Q} heterodimer incurred large CSPs as a function of pH (Figure 3a, b). Residues in the vicinity of monomer A (Gly9_A, Ala10_A, Gly17_A) displayed nearly identical CSPs as the EmrE-EmrE^{L51I} heterodimer, while residues near Glu14 in monomer B (Gly9_B, Ala10_B, Gly17_B) also displayed significant CSPs. However, we did not observe non-linear CSPs for monomer B residues like in the EmrE-EmrE^{L51I} heterodimer experiment. Notably, Gly17_B showed a linear CSP in EmrE-EmrE^{E14Q} pH titrations (Figure 3b), which contrasted with the striking non-linear CSP observed in the EmrE-EmrE^{L51I} titration (Figure 2b). A single pK_a value adequately fit all CSP data for EmrE-EmrE^{E14Q}, in agreement with the single Glu14 in the dimer (Figure 3c, d). These fits yielded a pK_a value of 7.2 ± 0.1 , which was in quantitative agreement with the more acidic pK_a value determined from EmrE-EmrE^{L51I} heterodimer experiments.

We also compared chemical shift changes between pH 5.0 and 10.0 for residues in the heterodimers with one Glu14 (EmrE-EmrE^{E14Q}) or two Glu14 residues (EmrE-EmrE^{L51I}) (Figure 4a, b). The correlation plots displayed slopes of 0.90 ± 0.06 for monomer A residues and 0.57 ± 0.08 for monomer B residues (Figure 4c). The slope close to unity for monomer A suggested a strong similarity of conformational changes in monomer A for dimers with one or two protonatable Glu14 residues (i.e., EmrE-EmrE^{L51I}). A larger deviation from unity was observed for the slopes of monomer B peaks and indicated deprotonation of Glu14^B was responsible for additional CSPs within monomer B, such as Ala10_B and Gly67_B, relative to those in the EmrE-EmrE^{L51I} heterodimer (Figure 4b). However, CSPs plotted onto the structure of EmrE showed very similar profiles for EmrE-EmrE^{L51I} and EmrE-EmrE^{E14Q} heterodimers, albeit with a few

small differences around Glu14_B (Figure 4d). Overall, these results support the conclusion that deprotonation of Glu14 within monomer A serves as the primary site responsible for triggering a global conformational change in the EmrE dimer. Such a change may involve differences in solvent accessibility of the substrate binding site, which has been observed in molecular dynamics simulations (22).

Glu14 residues are not electrostatically coupled

Two pK_a values raised the question whether the Glu14 residues in the dimer are electrostatically coupled (21). If coupling existed, deprotonation at one Glu14 residue may increase or decrease the apparent pK_a value of the other Glu14 site. By contrast, if Glu14 sites were uncoupled, each Glu14 would have an independent pK_a value that would not depend on the protonation state of the other. Heterodimer experiments in Figures 2 and 3 provided clues about the coupling mechanism since the pK_a value of 7.2 for Glu14_A of EmrE-EmrE^{E14Q} matched the more acidic pK_a value in the EmrE heterodimer with two Glu14 residues (8).

We hypothesized that a heterodimer of EmrE and the double mutant EmrE^{E14Q, L51I} would allow us to estimate the pK_a value for Glu14_B in the absence of a protonatable site within monomer A (Figure 5a). Hence, we mixed isotopically enriched EmrE with excess EmrE^{E14Q, L51I} at natural abundance and acquired ¹H/¹⁵N TROSY spectra at different pH values (Figure 5b, c; Supplemental Figure 5). We observed intense monomer B peaks at pH < 8.5 and intense monomer A peaks at pH ≥ 8.5, supporting a change in the conformational equilibrium around this pH value. These data indicated that the L51I mutation of EmrE^{E14Q, L51I} influenced the equilibrium when Glu14 in the EmrE monomer was protonated, favoring EmrE as monomer B in the heterodimer. Conversely, deprotonated Glu14 in the EmrE monomer elicited a stronger

preference, favoring EmrE as monomer A in the heterodimer. Thus, the pK_a value could be estimated at the pH value where monomers A and B were equally populated. In addition to these intensity changes, we observed CSPs from pH 6.3 to 8.5 within monomer B peaks of EmrE in the heterodimer (Figure 5b, c). These perturbations were consistent with a two-step process involving a fast step followed by a slow step, where the fast step corresponded to proton binding/unbinding within monomer B and the slow step to conformational exchange to monomer A in the heterodimer (Figure 5a).

The population of EmrE in monomer B (p_B) was calculated by analyzing the intensities of monomer A and B peaks for residues in proximity to Glu14 as a function of pH (Figure 5d). These populations were fitted to a modified Henderson-Hasselbalch equation and gave a pK_a value of 8.3 ± 0.1 for Glu14_B. This pK_a value was in good agreement with the more basic pK_a value (8.4 ± 0.2) observed in EmrE-EmrE^{L51I} experiments. Hence, pK_a values determined for Glu14_A and Glu14_B in heterodimers containing a single Glu14 residue were consistent with the two pK_a values observed for heterodimers containing two Glu14 residues. This observation indicates the presence of independent pK_a values and the absence of electrostatic coupling. These results also imply that Glu14 residues are somewhat distant inside the substrate binding pocket or that the presence of water screens the charges on the glutamate residues (22, 23). Although there is no experimental structure of proton-bound EmrE ($E_A^H-E_B^H$), molecular dynamics simulations performed on this state displayed an average distance between the two Glu14 residues of 13.6 Å (Supplemental Figure 6) (22). Such a distance exceeds those found in typical electrostatic interactions (24, 25) and supports experimental NMR measurements indicating the absence of electrostatic coupling between Glu14 residues. Finally, these results

underscore that the two pK_a values arise from different conformations in the asymmetric EmrE dimer and not from electrostatic coupling.

Discussion

EmrE's transport cycle requires the presence of proton and drug bound forms and conformational exchange between inward-open and outward-open states. Here, we determined E_A^- - E_B^H to be the most populated conformer of drug-free EmrE under pH conditions found in the cytoplasm of *E. coli* (pH \sim 7.5). We hypothesize this state plays a central role in the transport cycle since it can bind a drug substrate, bind to a proton at Glu14_A, or undergo deprotonation at Glu14_B. Unlike the other drug-free states of EmrE (E_A^H - E_B^H and E_A^- - E_B^-), E_A^- - E_B^H has different protonation states at the two Glu14 residues in the dimer. Hence, if exchange occurred between inward-open and outward-open states of E_A^- - E_B^H , the proton would transfer from one monomer to the other during the conformational change (Figure 6a). As a result, this *proton hopping mechanism* would rapidly dissipate a pH gradient across a membrane. Notably, the conformational exchange rate accompanying proton hopping was set to 100 sec⁻¹, which is \sim 14-fold faster than conformational exchange when EmrE is drug bound (7.3 sec⁻¹) (9). This indicates that proton hopping would not be the rate limiting step in the transport cycle. This mechanism is a central feature of the *free exchange model* of EmrE and simulations of the transport cycle required the inclusion of fixed concentrations of protons on both sides of the membrane to prevent proton leakage predicted by the model (9). Yet, EmrE and other SMR family members do not leak protons (9, 26, 27), suggesting conformational exchange occurs when EmrE is bound to a drug substrate or both protons at Glu14. Furthermore, independent pK_a values measured for Glu14 residues in this work and the relatively long distance between Glu14

residues in molecular dynamics simulations (22, 23) suggests no significant electrostatic coupling between the two anionic residues within the substrate binding pocket, which would be expected from an efficient proton transfer process. Taken together, these observations imply that an alternative mechanism is needed to explain the ion-coupled transport cycle for EmrE.

Here, we propose a *hop-free model* where conformational exchange and proton transfer do not occur simultaneously (Figure 6b). This mechanism is consistent with NMR observations that detected no electrostatic coupling between the Glu14 residues. In the hop-free model, inward-open E_A^- - E_B^H exchanges with outward-open E_A^H - E_B^- and outward-open E_A^- - E_B^H exchanges with inward-open E_A^H - E_B^- . In contrast to exchange in the proton hopping model, the free energies of exchanging states are different in our model. Indeed, conformational exchange of E_A^- - E_B^H to E_A^H - E_B^- is strongly disfavored since the relative free energy of E_A^H - E_B^- is higher than E_A^- - E_B^H . We estimated this free energy difference at ~ 2.9 kcal/mol using EmrE-EmrE^{E14Q} heterodimer experiments (see Materials and Methods), which reduces the probability of exchange and therefore proton leakage.

The hop-free mechanism is consistent with two key observations in the literature. First, growth inhibition assays in *E. coli* showed that heterodimers of EmrE-EmrE^{E14Q} do not confer drug resistance (19, 28). We found that EmrE-EmrE^{E14Q} displayed a biased conformational equilibrium that would halt the transport cycle and account for the ablated phenotype. This explanation is consistent with the correlation we established between the inward-open/outward-open conformational equilibrium and reduced growth inhibition in *E. coli* (19). Hence, the hop-free model is not in conflict with the EmrE-EmrE^{E14Q} growth inhibition data but rather explains these observations with a biased conformational equilibrium.

Second, conformational exchange experiments performed on wild-type EmrE showed decreased exchange rates from acidic to basic pH values (8). These data suggest significantly slower exchange for $E_A^- \cdot E_B^H$ and $E_A^- \cdot E_B^-$ relative to $E_A^H \cdot E_B^H$. However, due to the relatively small difference in pK_a values for the two Glu14 residues, it is not possible to directly measure the exchange rate for $E_A^- \cdot E_B^H$ in the absence of contributions from $E_A^- \cdot E_B^-$ or $E_A^H \cdot E_B^H$. Therefore, the exchange measurements do not prove the existence of conformational exchange and proton hopping between inward-open $E_A^- \cdot E_B^H$ and outward-open $E_A^- \cdot E_B^H$. These previous measurements are consistent with the hop-free mechanism.

Using our findings and others reported in the literature, we propose the transport model in Figure 7 and explain the steps as follows. Step 1, inward-open $E_A^H \cdot E_B^H$ deprotonates at Glu14_A to form $E_A^- \cdot E_B^H$ under cytoplasmic pH conditions of *E. coli*. Step 2, drug binds to $E_A^- \cdot E_B^H$, forming $E_A^- \cdot E_B^H$ -drug. Step 3, drug binding induces a more acidic pK_a value for Glu14_B, favoring formation of $E_A^- \cdot E_B^-$ -drug (9). Step 4, conformational exchange from inward-open $E_A^- \cdot E_B^-$ -drug to the outward-open state moves the drug from the cytoplasmic to periplasmic side of the membrane. Step 5, Glu14_B protonates at acidic pH values in the periplasm in *E. coli*, resulting in $E_A^- \cdot E_B^H$ -drug. Step 6, drug is released, which occurs at a faster rate for $E_A^- \cdot E_B^H$ -drug than $E_A^- \cdot E_B^-$ -drug (29). Step 7, outward-open $E_A^- \cdot E_B^H$ protonates Glu14_A to form $E_A^H \cdot E_B^H$. Step 8, conformational exchange switches outward-open $E_A^H \cdot E_B^H$ to the inward-open state. The preferred pathway in this model reduces proton leakage since exchange between $E_A^- \cdot E_B^H$ and $E_A^H \cdot E_B^-$ is unfavorable both for the inward-open and outward-open conformations.

In conclusion, we discovered that the asymmetric structure of EmrE and not the presence of electrostatic coupling determines the two pK_a values of Glu14 in the dimer. Thus, in the absence of proton hopping, we propose the energy difference between the two singly proton

bound states ($E_A^- \cdot E_B^H$ and $E_A^H \cdot E_B^-$) reduces the probability of conformational exchange and proton leakage. Since several transporters contain inverted repeat domains and essential anionic residues similar to EmrE (30-32), the hop-free model may explain the lack of proton leakage in other secondary active transporters. The hop-free mechanism can also be considered with the membrane potential which may further reduce proton leak cycles to conserve energy for uphill transport (33).

Materials and Methods

Protein expression and purification

Expression and purification of EmrE was performed as previously reported (8, 16, 17, 34). Briefly, EmrE was expressed as a fusion construct with maltose-binding protein in BL21(DE3) *E. coli* and purified using affinity and size exclusion chromatography in n-dodecyl- β -D-maltopyranoside (DDM, Anatrace). For solid-state NMR experiments, isotopically labeled EmrE was expressed in minimal media (M9) with $^{13}\text{C}_6$ glucose and ^{15}N ammonium chloride, while unlabeled EmrE was expressed in LB media. For solution NMR experiments, isotopically enriched EmrE was expressed in M9 media with perdeuterated glucose and ^{15}N ammonium chloride, while unlabeled EmrE was expressed in M9 media with perdeuterated glucose and natural abundance ammonium chloride. EmrE mutants of EmrE^{E14Q}, EmrE^{L51I}, and EmrE^{E14Q, L51I} were constructed using site directed mutagenesis and expressed in the same manner as described above.

NMR sample preparation

Preparation of heterodimer samples, EmrE-EmrE^{L51I} or EmrE-EmrE^{E14Q} or EmrE-EmrE^{E14Q, L51I}, involved mixing an isotopically labeled protein with an unlabeled protein at a ratio of 1/1.6 (mol/mol). The mixture was incubated in DDM and 50 mM DTT for 1 hr at 37 °C (19).

For solid-state NMR samples, EmrE was reconstituted into 1,2-di-*O*-tetradecyl-sn-glycero-3-phosphocholine (*O*-14:0-PC) (Avanti Polar Lipids) at a lipid to protein ratio of 30/1 (mol/mol). DDM detergent was removed by addition of Bio-Beads SM-2 resin (Bio-Rad) in a 100-fold excess relative to DDM (w/w). Proteoliposomes in 150 mM sodium phosphate and 20 mM sodium chloride were ultracentrifuged for 12 hours at 436,000 x g using a TLA-100 rotor

(Beckman-Coulter). The proteoliposome pellet was packed into a 3.2mm MAS rotor using sample spacers to prevent dehydration. To change the pH, the samples were buffer exchanged by resuspending proteoliposomes at pH 5.0, 8.0, or 10.0, performing freeze-thaw cycles, and ultracentrifuging.

For solution NMR samples, EmrE was reconstituted into dimyristoyl-sn-glycero-3-phosphocholine/dihexanoyl-sn-glycero-3-phosphocholine (DMPC/DHPC) with the perdeuterated chains (14:0 PC D54 and 6:0 PC D22, Cortecnet) to make isotropic bicelles ($q = 0.33$). The DMPC lipid to protein ratio was 30/1 (mol/mol). The final heterodimer samples contained 1.39 mM total protein and homodimer sample contained 0.533 mM protein. The solution NMR buffer was 150 mM sodium phosphate, 20 mM sodium chloride, and 10% deuterium oxide.

Solid-state NMR spectroscopy

Solid-state NMR spectra were recorded on an Agilent DD2 NMR spectrometer operating at a ^1H frequency of 600 MHz (14.1 T) equipped with a 3.2 mm triple resonance MAS probe manufactured by Black Fox, LLC. The sample temperature was set to -20 °C or -5 °C with an MAS rate at 8333 ± 5 Hz or 12500 ± 5 Hz. Typical 90° pulse lengths of ^1H , ^{13}C and ^{15}N nuclei were 2.5, 4.5 and 5 μs , respectively. ^1H - ^{13}C / ^{15}N cross-polarization used radiofrequency (RF) pulses of 55.6 (or 50 kHz) for ^{13}C (or ^{15}N) with a tangent ramp (35) on ^1H . Frequency selective polarization transfers from ^{15}N to ^{13}CA were carried out using SPECIFIC-CP (36) with a 5.5 ms tangent ramp on ^{13}C and with RF amplitudes of ~18.8, ~31.3 and 110 kHz on ^{15}N , ^{13}C , and ^1H , respectively. The ^1H RF power was set to 100 kHz for decoupling during acquisition and evolution periods.

For double-quantum single-quantum experiments, an SPC-5 pulse (37) with 1.2 ms Z-filtered time was used for the conversion and reconversion steps. During the SPC-5 element, continuous wave ^1H decoupling with RF of 100 kHz was used. REDOR dephasing of ^{15}N in the DQSQ-REDOR experiment was achieved by a composite 90°-180°-90° pulse train (38) using a 5 μs 90° pulse. The chemical shifts of ^{13}C and ^{15}N were indirectly calibrated by external referencing the CH_2 resonance of adamantane to 40.48 ppm (39). All the multidimensional NMR spectra were processed in NMRPipe (40) and analyzed using Sparky (41).

Solution NMR spectroscopy

Solution NMR spectra were acquired at 37 °C on a Bruker spectrometer operating at a ^1H frequency of 600 MHz (14.1 T) equipped with a triple resonance TCI cryogenic probe. For pH titrations, 2D $^1\text{H}/^{15}\text{N}$ TROSY experiments were recorded with spectral widths of 12,019.2 Hz and 1,520.6 Hz for ^1H and ^{15}N , respectively. The acquisition (^1H) and evolution times (^{15}N) were 59.9 msec and 22.8 msec. The pH stability of NMR samples was monitored before and after each TROSY experiment; the pH fluctuated by ± 0.02 . The total experimental time was ~ 1.5 days to complete the full pH titration curve. Residues with significant chemical shift perturbations, defined as $^1\text{H} > 0.03$ ppm and $^{15}\text{N} > 0.3$ ppm, were fitted in a global manner using a macroscopic two $\text{p}K_a$ model (equation 1) (42) or a one $\text{p}K_a$ model (equation 2).

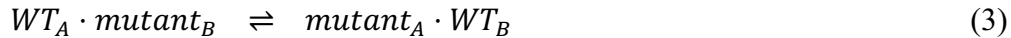
$$\delta = \frac{\delta_{\text{H}_2\text{A}} + \delta_{\text{HA}} 10^{\text{pH} - \text{p}K_{a,1}} + \delta_{\text{A}} 10^{[2\text{pH} - (\text{p}K_{a,1} + \text{p}K_{a,2})]}}{1 + 10^{(\text{pH} - \text{p}K_{a,1})} + 10^{[2\text{pH} - (\text{p}K_{a,1} + \text{p}K_{a,2})]}} \quad (1)$$

$$\delta = \frac{\delta_{\text{HA}} + \delta_{\text{A}} 10^{\text{pH} - \text{p}K_a}}{1 + 10^{\text{pH} - \text{p}K_a}} \quad (2)$$

$\delta_{\text{H}_2\text{A}}$, δ_{HA} and δ_{A} are the chemical shifts of the fully protonated, half-protonated and deprotonated states, respectively, in Equation 1. δ is the observed chemical shift. δ_{HA} and δ_{A} are the chemical shifts of the protonated and deprotonated states, respectively, in Equation 2.

Quantification of free energies from heterodimer samples

Determination of populations, equilibrium constants, and free energies for EmrE heterodimers have been described previously (19). In brief, the equilibrium for wild-type EmrE in a heterodimer with a mutant is given in Equation 3, where subscripts refer to monomer A or B in the dimer:



Populations of wild-type EmrE occupying monomer A (p_A) or monomer B (p_B) in the heterodimer are calculated using Equation 4:

$$\frac{I_{A,obs}}{I_{B,obs}} = \frac{I_A}{I_B} \frac{(f_{homo} + f_{het} p_A)}{(f_{homo} + f_{het} p_B)} \quad (4)$$

$I_{A,obs}$ and $I_{B,obs}$ are the observed ratio of intensities of monomer A and B peaks in a heterodimer spectrum, respectively. I_A and I_B are the intensities of monomer A and B peaks from a homodimer reference spectrum, which is needed since A and B peaks are not intrinsically the same. f_{homo} and f_{het} is the fraction of homodimers and heterodimers formed by the isotopically labeled protein in preparation of the heterodimer samples; f_{homo} and f_{het} were 0.24 and 0.76, respectively, by assuming statistical mixing of the 1/1.6 molar ratio of isotopically labeled and unlabeled proteins. Addition of p_A and p_B is equal to 1 and their ratio gives the equilibrium constant. The free energies reported are calculated from the equilibrium constant.

$I_{A,obs}$ and $I_{B,obs}$ were measured for resolved isoleucine methyl peaks (${}^{-13}\text{C}^{\delta}\text{H}_3$) in HMQC spectra corresponding to the isotopically enriched protein in the heterodimer: Ile11, Ile54, Ile58, Ile62, Ile68, Ile88, and Ile101 for EmrE-EmrE^{L51I}; Ile62, Ile68, Ile88, and Ile100 for EmrE-EmrE^{E14Q}; Ile16, Ile54, Ile58, and Ile101 for EmrE-EmrE^{E14Q, L51I}. I_A and I_B were measured for the same isoleucine methyl peaks of wild-type EmrE. The free energy of the conformational

preference of EmrE-EmrE^{E14Q} heterodimers at a pH value of 6.2 was estimated as the difference in the free energy of EmrE-EmrE^{E14Q, L51I} and EmrE-EmrE^{L51I}. This value of ~0.6 kcal/mol at pH 6.2 was subtracted from the free energy of the conformational preference of EmrE-EmrE^{E14Q} heterodimers at pH 9.5 (~3.5 kcal/mol) to give the intrinsic free energy difference between E_A⁻-E_B^H and E_A^H-E_B⁻ (~2.9 kcal/mol).

Acknowledgments

This work was supported by NIH (R01 AI108889) and NSF awards (MCB 1506420) to N.J.T. NMR data were collected using a cryoprobe that was supported by an NIH S10 grant (OD016343). We thank M. (Leninger) Crames for helpful discussions.

References

1. J. M. A. Blair, M. A. Webber, A. J. Baylay, D. O. Ogbolu, L. J. V. Piddock, Molecular mechanisms of antibiotic resistance. *Nature Reviews Microbiology* **13**, 42-51 (2015).
2. M. Saleh, D. C. Bay, R. J. Turner, Few Conserved Amino Acids in the Small Multidrug Resistance Transporter EmrE Influence Drug Polyselectivity. *Antimicrobial agents and chemotherapy* **62** (2018).
3. S. Schuldiner, EmrE, a model for studying evolution and mechanism of ion-coupled transporters. *Biochim Biophys Acta* **1794**, 748-762 (2009).
4. C. W. Sikora, R. J. Turner, Investigation of ligand binding to the multidrug resistance protein EmrE by isothermal titration calorimetry. *Biophys J* **88**, 475-482 (2005).
5. D. Rotem, S. Schuldiner, EmrE, a multidrug transporter from *Escherichia coli*, transports monovalent and divalent substrates with the same stoichiometry. *J Biol Chem* **279**, 48787-48793 (2004).
6. H. Yerushalmi, M. Lebendiker, S. Schuldiner, EmrE, an *Escherichia coli* 12-kDa multidrug transporter, exchanges toxic cations and H⁺ and is soluble in organic solvents. *J Biol Chem* **270**, 6856-6863 (1995).
7. E. A. Morrison *et al.*, Antiparallel EmrE exports drugs by exchanging between asymmetric structures. *Nature* **481**, 45-50 (2011).
8. A. Gayen, M. Leninger, N. J. Traaseth, Protonation of a glutamate residue modulates the dynamics of the drug transporter EmrE. *Nat Chem Biol* **12**, 141-145 (2016).
9. A. E. Robinson, N. E. Thomas, E. A. Morrison, B. M. Balthazor, K. A. Henzler-Wildman, New free-exchange model of EmrE transport. *Proc Natl Acad Sci U S A* **114**, E10083-E10091 (2017).
10. D. Rotem, S. Steiner-Mordoch, S. Schuldiner, Identification of tyrosine residues critical for the function of an ion-coupled multidrug transporter. *J Biol Chem* **281**, 18715-18722 (2006).
11. Y. Elbaz, N. Tayer, E. Steinfels, S. Steiner-Mordoch, S. Schuldiner, Substrate-induced tryptophan fluorescence changes in EmrE, the smallest ion-coupled multidrug transporter. *Biochemistry* **44**, 7369-7377 (2005).
12. G. Platzer, M. Okon, L. P. McIntosh, pH-dependent random coil H-1, C-13, and N-15 chemical shifts of the ionizable amino acids: a guide for protein pK (a) measurements. *Journal of Biomolecular Nmr* **60**, 109-129 (2014).
13. J. Li, A. Sae Her, N. J. Traaseth, Site-specific resolution of anionic residues in proteins using solid-state NMR spectroscopy. *Journal of Biomolecular NMR* **74**, 355-363 (2020).
14. K. Schmidt-Rohr, K. J. Fritzsching, S. Y. Liao, M. Hong, Spectral editing of two-dimensional magic-angle-spinning solid-state NMR spectra for protein resonance assignment and structure determination. *J Biomol NMR* **54**, 343-353 (2012).
15. Y. J. Chen *et al.*, X-ray structure of EmrE supports dual topology model. *Proc Natl Acad Sci U S A* **104**, 18999-19004 (2007).
16. A. Gayen, J. R. Banigan, N. J. Traaseth, Ligand-induced conformational changes of the multidrug resistance transporter EmrE probed by oriented solid-state NMR spectroscopy. *Angew Chem Int Ed Engl* **52**, 10321-10324 (2013).
17. M. K. Cho, A. Gayen, J. R. Banigan, M. Leninger, N. J. Traaseth, Intrinsic conformational plasticity of native EmrE provides a pathway for multidrug resistance. *J Am Chem Soc* **136**, 8072-8080 (2014).

18. N. J. B. Traaseth, J. R.; Leninger, M., Exploring Transporters within the SMR Family Using Solid-State NMR Spectroscopy. *eMagRes* **4**, 551-559 (2015).
19. M. Leninger, A. Sae Her, N. J. Traaseth, Inducing conformational preference of the membrane protein transporter EmrE through conservative mutations. *Elife* **8** (2019).
20. R. Dastvan, A. W. Fischer, S. Mishra, J. Meiler, H. S. McHaourab, Protonation-dependent conformational dynamics of the multidrug transporter EmrE. *Proc Natl Acad Sci U S A* **113**, 1220-1225 (2016).
21. E. A. Morrison, A. E. Robinson, Y. Liu, K. A. Henzler-Wildman, Asymmetric protonation of EmrE. *J Gen Physiol* **146**, 445-461 (2015).
22. J. V. Vermaas, S. B. Rempe, E. Tajkhorshid, Electrostatic lock in the transport cycle of the multidrug resistance transporter EmrE. *Proc Natl Acad Sci U S A* **115**, E7502-E7511 (2018).
23. V. Ovchinnikov, T. A. Stone, C. M. Deber, M. Karplus, Structure of the EmrE multidrug transporter and its use for inhibitor peptide design. *Proc Natl Acad Sci U S A* **115**, E7932-E7941 (2018).
24. S. Kumar, R. Nussinov, Close-range electrostatic interactions in proteins. *Chembiochem* **3**, 604-617 (2002).
25. H. X. Zhou, X. Pang, Electrostatic Interactions in Protein Structure, Folding, Binding, and Condensation. *Chem Rev* **118**, 1691-1741 (2018).
26. H. Yerushalmi, S. Schuldiner, An essential glutamyl residue in EmrE, a multidrug antiporter from *Escherichia coli*. *The Journal of biological chemistry* **275**, 5264-5269 (2000).
27. A. A. Kermani, C. B. Macdonald, R. Gundepudi, R. B. Stockbridge, Guanidinium export is the primal function of SMR family transporters. *Proc Natl Acad Sci U S A* **115**, 3060-3065 (2018).
28. M. Rapp, S. Seppala, E. Granseth, G. von Heijne, Emulating membrane protein evolution by rational design. *Science* **315**, 1282-1284 (2007).
29. Y. Adam, N. Tayer, D. Rotem, G. Schreiber, S. Schuldiner, The fast release of sticky protons: Kinetics of substrate binding and proton release in a multidrug transporter. *Proceedings of the National Academy of Sciences* **104**, 17989 (2007).
30. O. Pornillos, G. Chang, Inverted repeat domains in membrane proteins. *FEBS Lett* **580**, 358-362 (2006).
31. O. Boudker, G. Verdon, Structural perspectives on secondary active transporters. *Trends Pharmacol Sci* **31**, 418-426 (2010).
32. D. Du *et al.*, Multidrug efflux pumps: structure, function and regulation. *Nat Rev Microbiol* **16**, 523-539 (2018).
33. X. C. Zhang, M. Liu, G. Lu, J. Heng, Thermodynamic secrets of multidrug resistance: A new take on transport mechanisms of secondary active antiporters. *Protein Sci* **27**, 595-613 (2018).
34. J. R. Banigan, A. Gayen, M. K. Cho, N. J. Traaseth, A structured loop modulates coupling between the substrate-binding and dimerization domains in the multidrug resistance transporter EmrE. *J Biol Chem* **290**, 805-814 (2015).
35. M. Baldus, D. G. Geurts, S. Hediger, B. H. Meier, Efficient N-15-C-13 polarization transfer by adiabatic-passage Hartmann-Hahn cross polarization. *J Magn Reson Ser A* **118**, 140-144 (1996).

36. M. Baldus, A. T. Petkova, J. H. Herzfeld, R. G. Griffin, Cross polarization in the tilted frame: assignment and spectral simplification in heteronuclear spin systems. *Mol Phys* **95**, 1197-1207 (1998).
37. M. Hohwy, C. M. Rienstra, C. P. Jaroniec, R. G. Griffin, Fivefold symmetric homonuclear dipolar recoupling in rotating solids: Application to double quantum spectroscopy. *Journal of Chemical Physics* **110**, 7983-7992 (1999).
38. M. H. Levitt, R. Freeman, Nmr Population-Inversion Using a Composite Pulse. *Journal of Magnetic Resonance* **33**, 473-476 (1979).
39. C. R. Morcombe, K. W. Zilm, Chemical shift referencing in MAS solid state NMR. *Journal of magnetic resonance (San Diego, Calif.: 1997)* **162**, 479-486 (2003).
40. F. Delaglio *et al.*, NMRPipe: a multidimensional spectral processing system based on UNIX pipes. *J Biomol NMR* **6**, 277-293 (1995).
41. T. D. Goddard, D. G. Kneller, SPARKY 3. *University of California, San Francisco*.
42. L. P. McIntosh *et al.*, Dissecting electrostatic interactions in *Bacillus circulans* xylanase through NMR-monitored pH titrations. *J Biomol NMR* **51**, 5-19 (2011).

Figure Legends

Figure 1. Detection of Glu14 chemical shifts in EmrE using solid-state NMR spectroscopy in lipid bilayers.

(a) DQSQ-REDOR spectra of uniformly $^{13}\text{C}/^{15}\text{N}$ labeled EmrE. (b) DQSQ-REDOR spectra of heterodimers composed of $^{13}\text{C}/^{15}\text{N}$ labeled EmrE $^{\text{L51I}}$ and natural abundance EmrE. (c) DQSQ-REDOR spectra of heterodimers composed of $^{13}\text{C}/^{15}\text{N}$ labeled EmrE and natural abundance EmrE $^{\text{L51I}}$. Each spectrum was collected at pH values of 5.0 (top row), 8.0 (middle row), and 10.0 (bottom row). The underlined protein indicates the isotopically enriched monomer in the heterodimer. The peak positions of protonated and deprotonated Glu14 residues are shown in red and blue boxes, respectively. Asterisks denote residual signals from backbone glycine residues.

Figure 2. Determination of $\text{p}K_a$ values for Glu14 residues in the EmrE-EmrE $^{\text{L51I}}$ heterodimer using solution NMR spectroscopy.

(a) $^1\text{H}/^{15}\text{N}$ TROSY spectra at the indicated pH values for heterodimers composed of isotopically enriched EmrE $^{\text{L51I}}$ and natural abundance EmrE. (b) $^1\text{H}/^{15}\text{N}$ TROSY spectra at the indicated pH values for heterodimers composed of isotopically enriched EmrE and natural abundance EmrE $^{\text{L51I}}$. (c, d) Chemical shifts as a function of pH for (c) monomer A and (d) monomer B. The dotted line is the global fit to the two- $\text{p}K_a$ model in Equation 1.

Figure 3. Determination of the $\text{p}K_a$ value for Glu14 in monomer A of the EmrE-EmrE $^{\text{E14Q}}$ heterodimer using solution NMR spectroscopy.

(a) $^1\text{H}/^{15}\text{N}$ TROSY spectra at the indicated pH values for heterodimers composed of isotopically enriched EmrE and natural abundance EmrE $^{\text{E14Q}}$. (b) $^1\text{H}/^{15}\text{N}$ TROSY spectra at the indicated pH values for heterodimers composed of isotopically enriched EmrE $^{\text{E14Q}}$ and natural abundance EmrE. (c, d) Chemical shifts as a function of pH for (c) monomer A and (d) monomer B. The dotted line is the global fit to the one- $\text{p}K_a$ model in Equation 2.

Figure 4. Chemical shift comparison for heterodimers comprised of one or two Glu14 residues.

(a) $^1\text{H}/^{15}\text{N}$ TROSY spectra of heterodimers at pH 5.0 (black) and pH 10.0 (red) for monomer A residues in EmrE-EmrE $^{\text{L51I}}$ (left, “two Glu14”) and EmrE-EmrE $^{\text{E14Q}}$ (right, “one Glu14”). (b) $^1\text{H}/^{15}\text{N}$ TROSY spectra of heterodimers at pH 5.0 (black) and pH 10.0 (red) for monomer B residues in EmrE-EmrE $^{\text{L51I}}$ (left, “two Glu14”) and EmrE-EmrE $^{\text{E14Q}}$ (right, “one Glu14”). (c) Correlation plots of the chemical shift difference ($\Delta\delta$) between pH 5.0 and pH 10.0 for residues in monomer A (left) and monomer B (right). The y-axis name, “two Glu14”, corresponds to the EmrE-EmrE $^{\text{L51I}}$ heterodimer, while the x-axis name, “one Glu14”, corresponds to the EmrE-EmrE $^{\text{E14Q}}$ heterodimer. (d) Combined $^1\text{H}/^{15}\text{N}$ CSPs between pH values of 5.0 and 10.0 plotted onto the EmrE structure (PDB: 3B5D (15)) for data derived from the EmrE-EmrE $^{\text{L51I}}$ (“two Glu14”) and EmrE-EmrE $^{\text{E14Q}}$ (“one Glu14”) heterodimers. The color range from blue to red corresponds to the smallest to largest CSPs, respectively. Arrows highlight differences in the CSP profiles.

Figure 5. Determination of the $\text{p}K_a$ value for Glu14 in monomer B of the EmrE-EmrE $^{\text{E14Q,L51I}}$ heterodimer using solution NMR spectroscopy.

(a) Cartoon representation of EmrE-EmrE^{E14Q,L51I} heterodimer experiments where “H⁺” and “-” refer to protonated and deprotonated Glu14, respectively. (b, c) ¹H/¹⁵N TROSY spectra of isotopically enriched EmrE in the EmrE-EmrE^{E14Q, L51I} heterodimer (black). The superimposed spectra in blue and red correspond to monomer B peaks at pH 6.3 (blue) and monomer A peaks at pH 9.0 (red) as measured from the EmrE-EmrE^{L51I} heterodimer sample. (d) Population of monomer B (p_B) in the EmrE-EmrE^{E14Q,L51I} heterodimer calculated by dividing the intensity of monomer B peaks by the sum of intensities of monomer A and B peaks. The fitted line indicates the pK_a value for Glu14 of monomer B.

Figure 6. Conformational exchange mechanisms displaying (a) proton hopping and (b) no proton hopping.

Monomer A or B are indicated within each subunit; “H⁺” and “-” correspond to protonated or deprotonated Glu14, respectively. The hopping mechanism leads to significant proton leak, while the hop-free mechanism reduces proton leak.

Figure 7. Model of proton-coupled drug efflux by EmrE.

Monomer A or B are indicated and “H⁺” or “-” within each monomer correspond to protonated or deprotonated Glu14, respectively; the drug is indicated with a “D”. The equilibria are indicated by numbers and are referenced in the text. Asterisks correspond to the E_A^- - E_B^H inward-open (top) and outward-open conformations (bottom); exchange between these conformations results in a proton leak cycle (see Figure 6a) and is disallowed for efficient exchange.

Figure 1

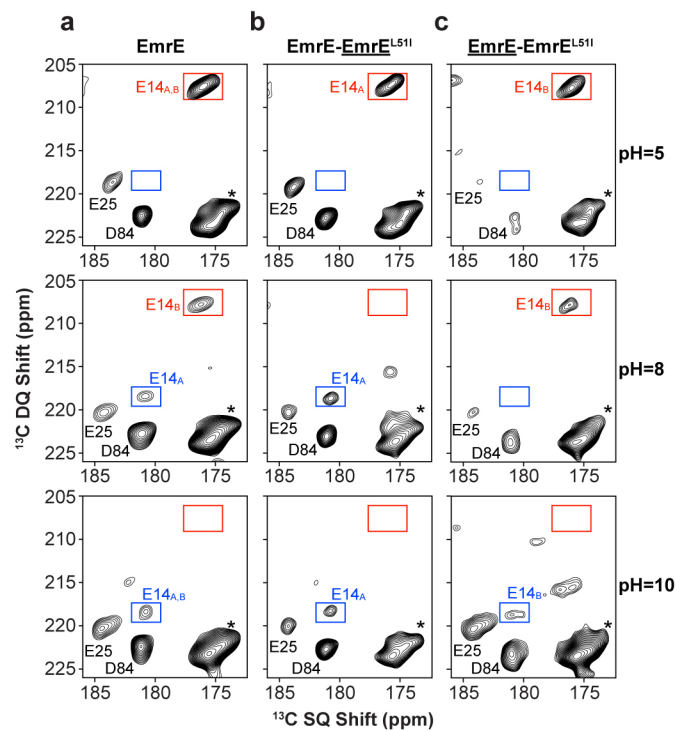


Figure 2

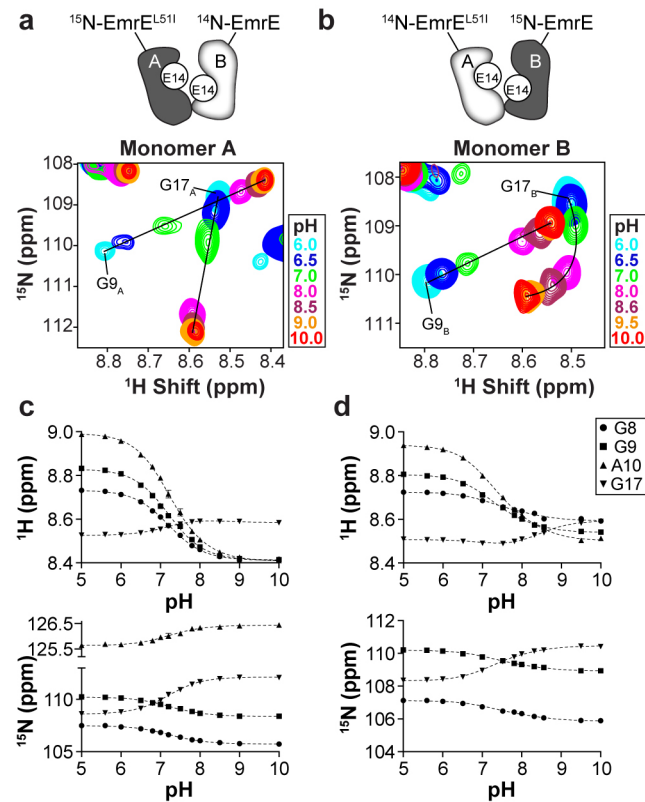


Figure 3

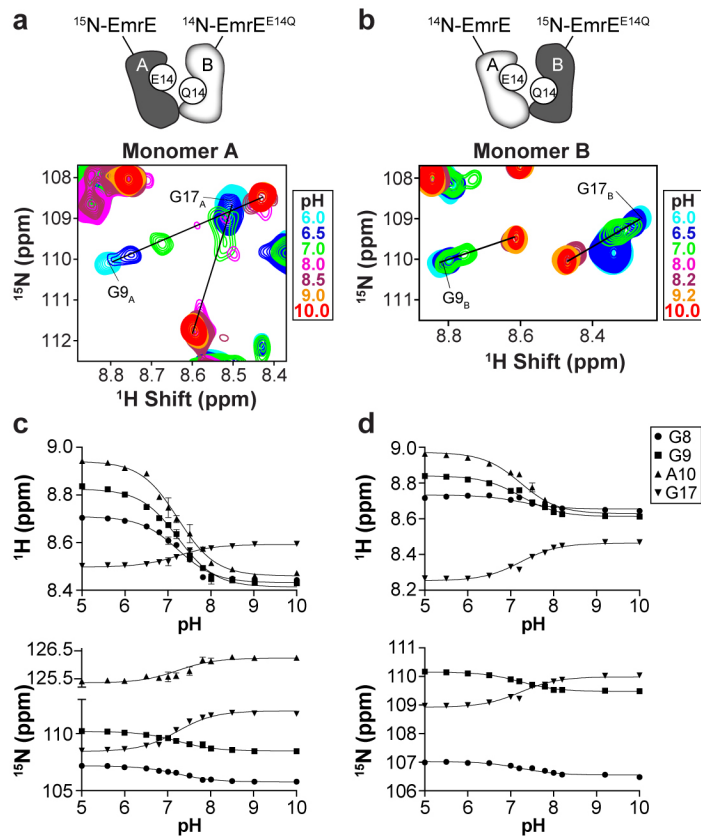


Figure 4

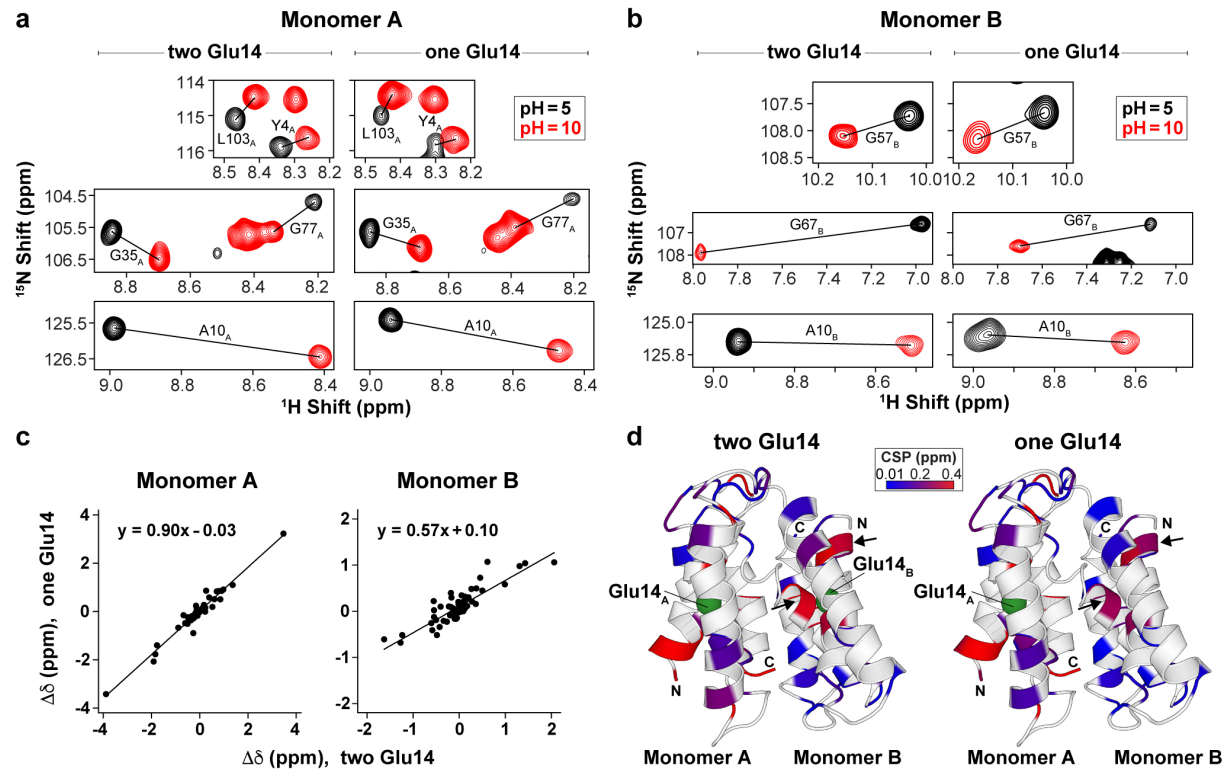


Figure 5

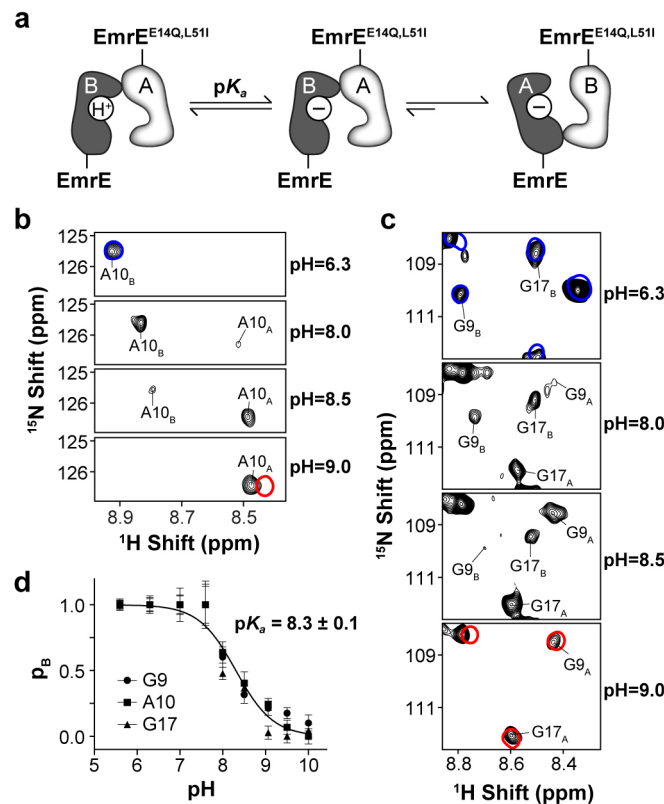


Figure 6

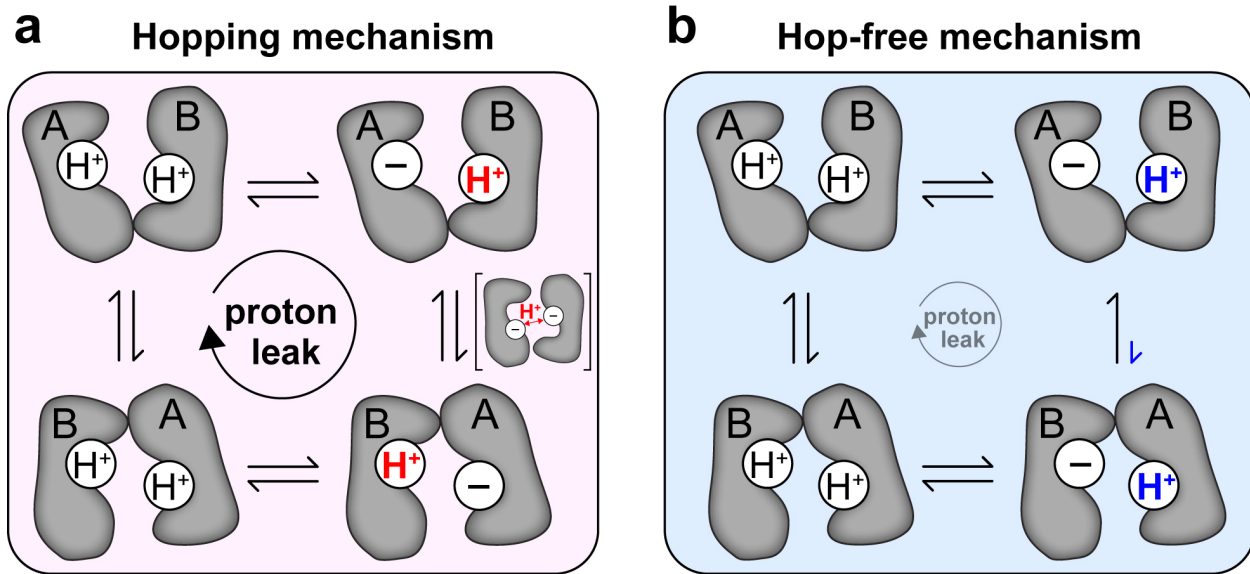
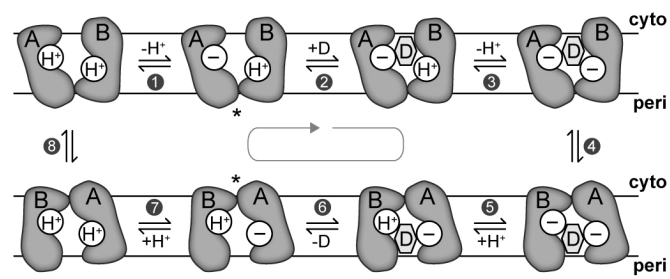


Figure 7



Supplementary Information

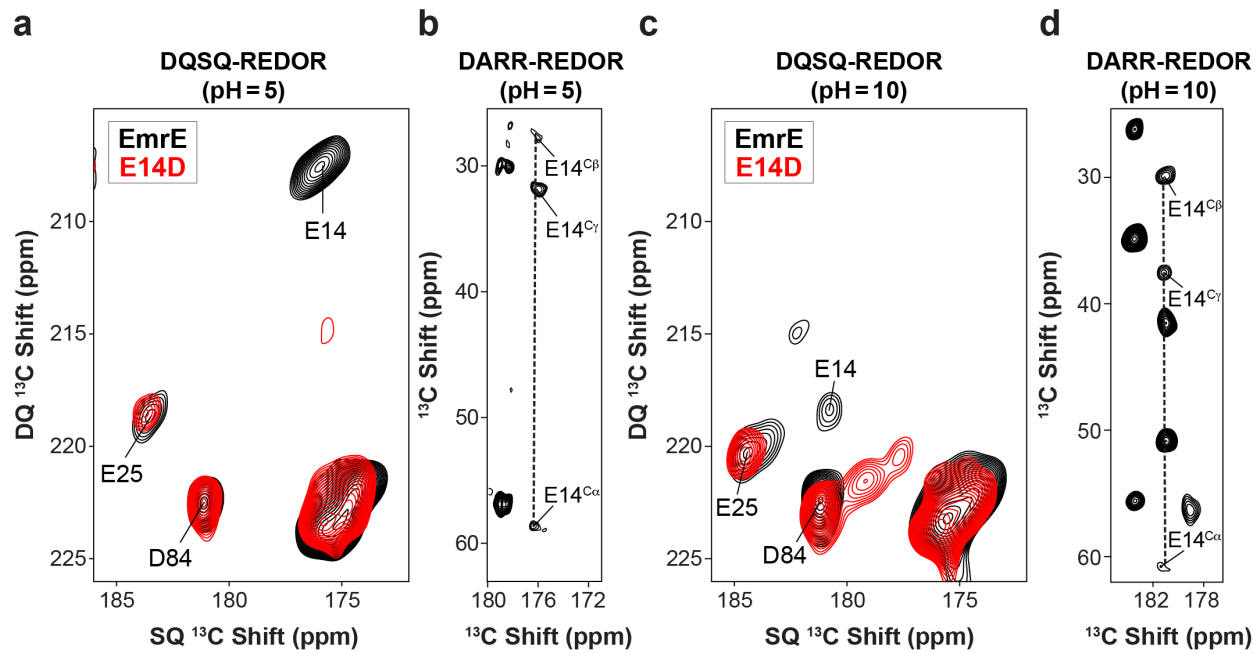
Asymmetric protonation of glutamate residues drives a preferred transport pathway in EmrE

Jianping Li⁺, Ampon Sae Her⁺, Nathaniel J. Traaseth*

Department of Chemistry, New York University, New York, NY 10003

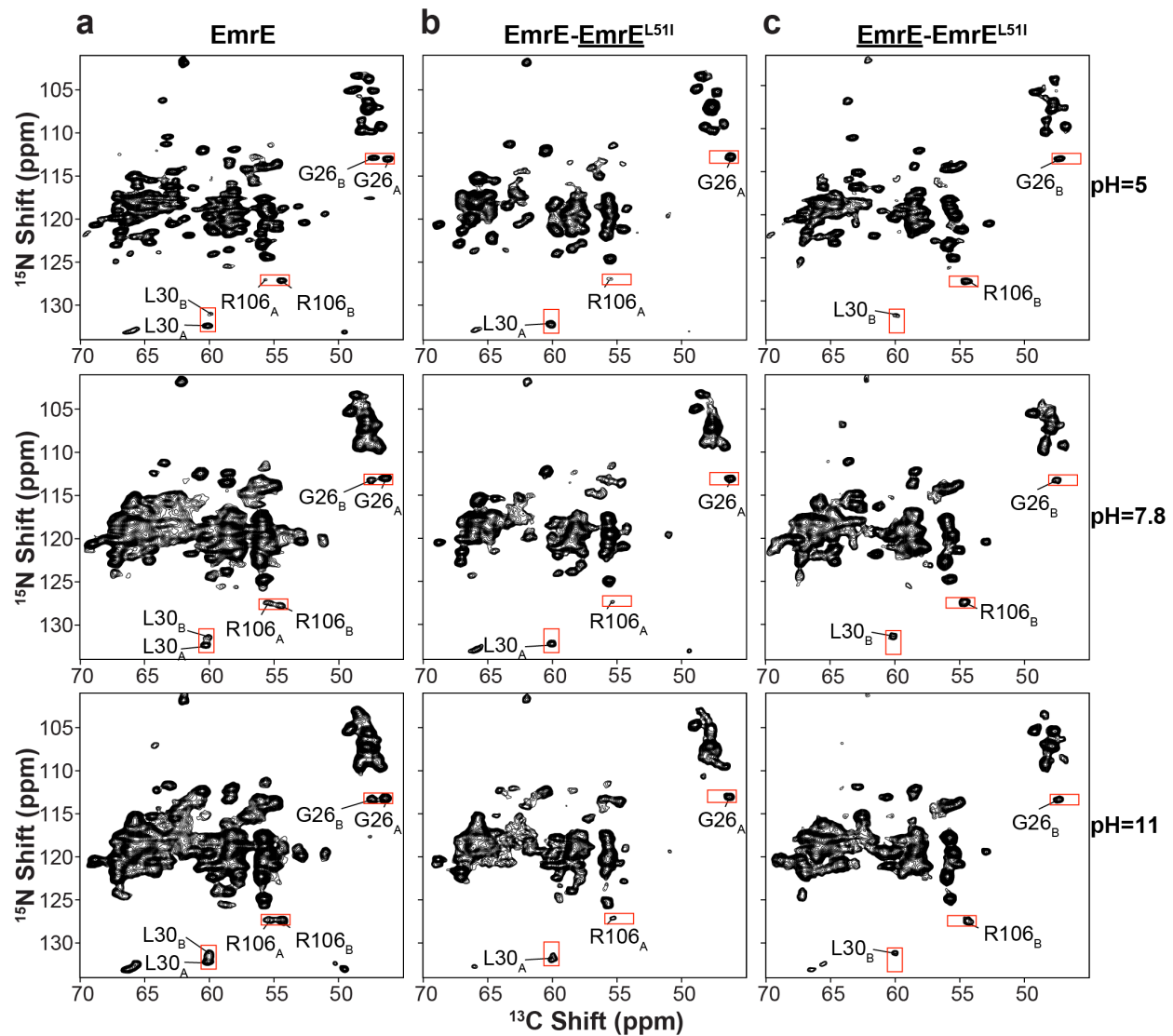
⁺ These authors contributed equally to this work

* Corresponding author: traaseth@nyu.edu



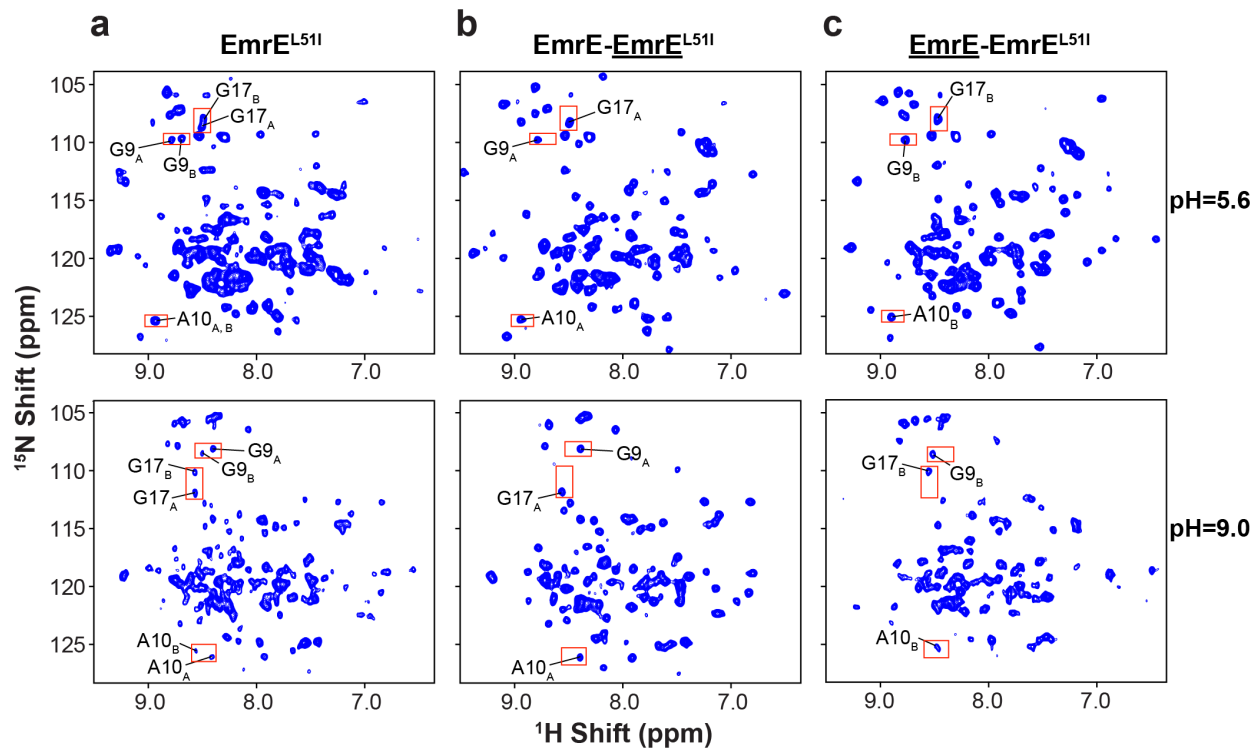
Supplemental Figure 1. Solid-state NMR assignment of Glu14 in wild-type EmrE using mutagenesis and REDOR-DARR spectra.

(a) DQSQ-REDOR spectra of wild-type EmrE (black) and E14D (red) with 1.2 ms REDOR dephasing at pH 5.0. (b) REDOR-DARR (1) spectrum of wild-type EmrE with 4.5 ms REDOR dephasing showing side chain chemical shifts of Glu14 at pH 5.0. (c) DQSQ-REDOR spectra of wild-type EmrE (black) and E14D (red) with 1.2 ms REDOR dephasing at pH 10.0. (d) REDOR-DARR spectrum of wild-type EmrE with 3.8 ms REDOR dephasing showing side chain chemical shifts of Glu14 at pH = 10.0.



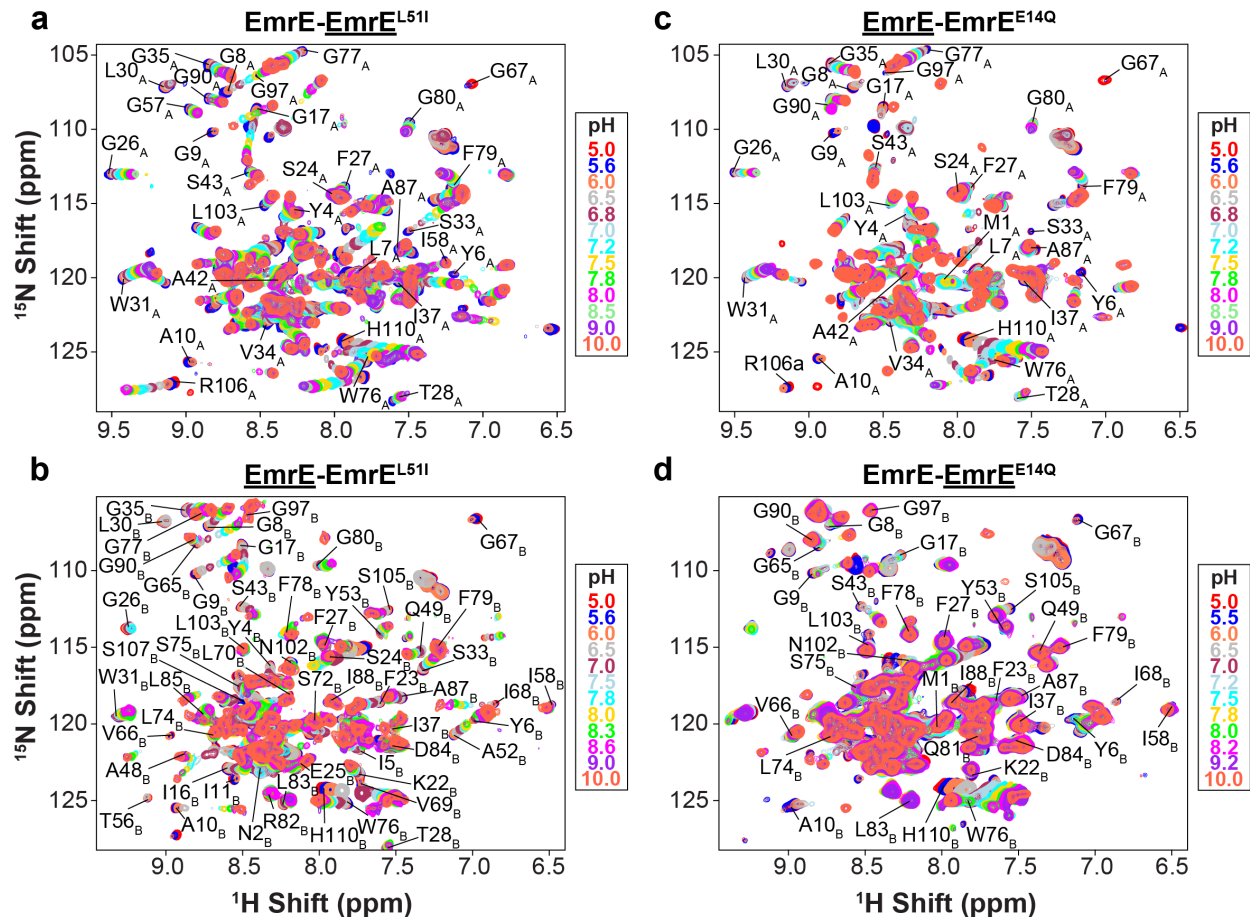
Supplemental Figure 2. The EmrE-EmrE^{L51I} heterodimer displays a conformational bias as detected using solid-state NMR experiment.

NCA correlation spectra for (a) ¹⁵N, ¹³C wild-type EmrE, (b) heterodimer of ¹⁵N, ¹³C EmrE^{L51I} and natural abundance wild-type EmrE, and (c) heterodimer of ¹⁵N, ¹³C EmrE and natural abundance EmrE^{L51I} acquired at pH values of 5.0 (top), 7.8 (middle), and 11.0 (bottom). The peaks of Gly26, Leu30 and Arg106 are highlighted with red rectangles.



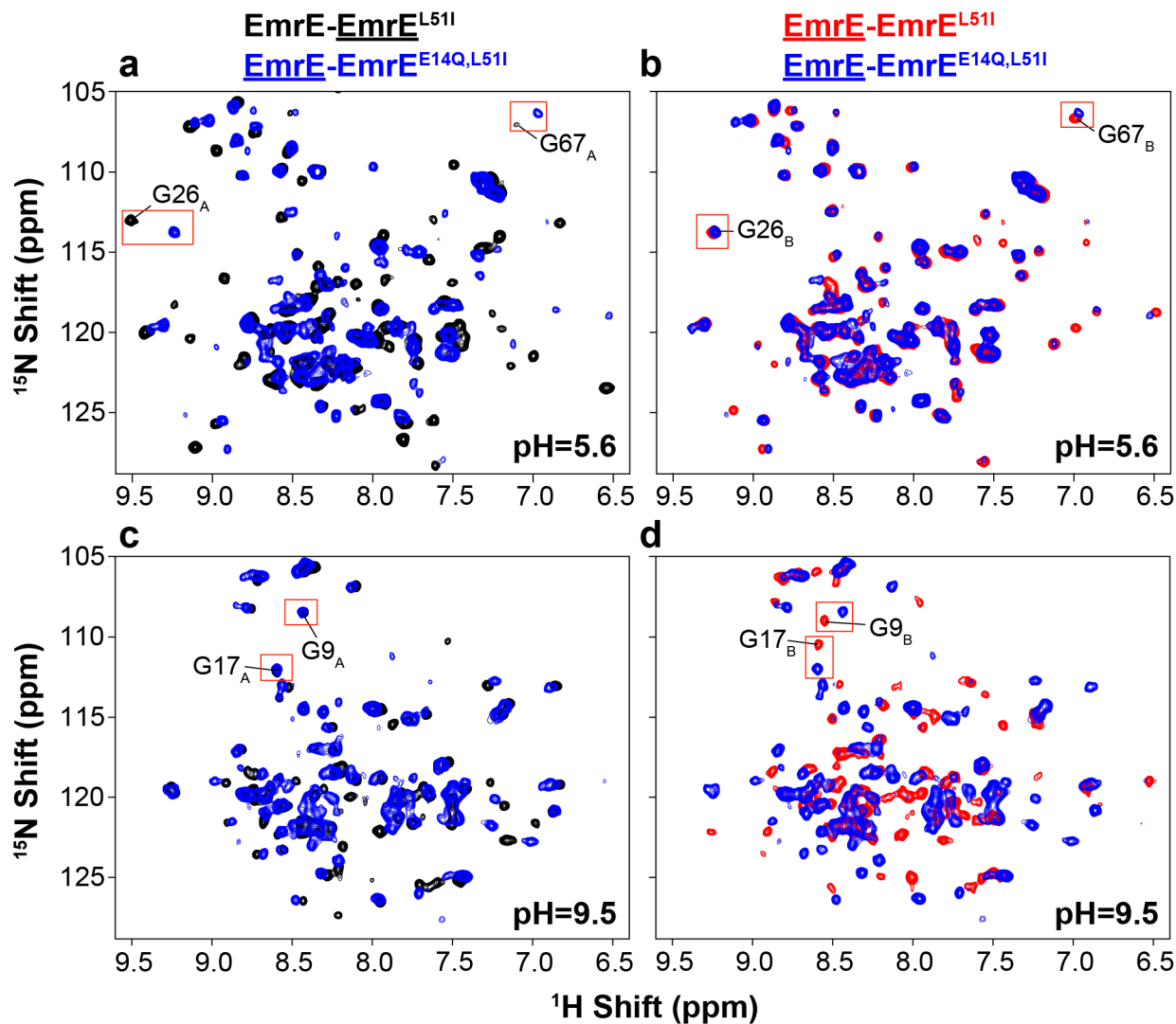
Supplemental Figure 3. Backbone $^1\text{H}/^{15}\text{N}$ TROSY spectra of EmrE heterodimers display a conformational bias.

$^1\text{H}/^{15}\text{N}$ TROSY solution NMR spectra of (a) ^{15}N labeled EmrE $^{\text{L51I}}$, (b) heterodimer of ^{15}N labeled EmrE $^{\text{L51I}}$ and natural abundance EmrE, (c) heterodimer of ^{15}N labeled EmrE and natural abundance EmrE $^{\text{L51I}}$ acquired at pH values of 5.6 (top) and pH 9.0 (bottom). The peaks of Gly9, Ala10 and Gly17 are highlighted with red rectangles.



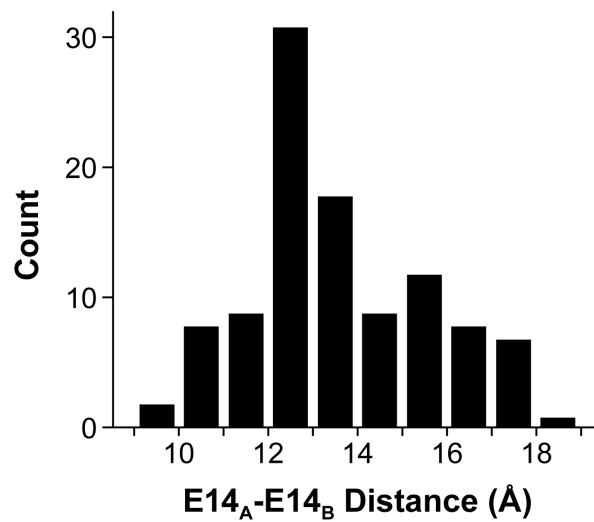
Supplemental Figure 4. $^1\text{H}/^{15}\text{N}$ TROSY spectra of pH titration experiments for each heterodimer sample.

¹H/¹⁵N TROSY solution NMR spectra of heterodimers corresponding to: (a) ¹⁵N labeled EmrE^{L51I} and unlabeled EmrE, (b) ¹⁵N labeled EmrE and unlabeled EmrE^{L51I}, (c) ¹⁵N labeled EmrE and unlabeled EmrE^{E14Q}, (d) ¹⁵N EmrE^{E14Q} and unlabeled EmrE. Panels (a) and (c) show a conformational preference for monomer A, while panels (b) and (d) show a preference for monomer B.



Supplemental Figure 5. The EmrE-EmrE $^{\text{E}14\text{Q,L}51\text{I}}$ heterodimer displays a different conformational preference at acidic and basic pH values.

(a, c) Overlay of $^1\text{H}/^{15}\text{N}$ TROSY spectra of a heterodimer of ^{15}N labeled EmrE and unlabeled EmrE $^{\text{E}14\text{Q,L}51\text{I}}$ (blue) and a heterodimer of ^{15}N labeled EmrE $^{\text{L}51\text{I}}$ and unlabeled EmrE (black) at pH values of 5.6 (a) and 9.5 (c). (b, d) Overlay of $^1\text{H}/^{15}\text{N}$ TROSY spectra of a heterodimer of ^{15}N labeled EmrE and unlabeled EmrE $^{\text{E}14\text{Q,L}51\text{I}}$ (blue) and a heterodimer of ^{15}N labeled EmrE and unlabeled EmrE $^{\text{L}51\text{I}}$ (red) at pH values of 5.6 (b) and 9.5 (d). The overlaid spectra in panel (b) are more similar than in panel (a), indicating that the EmrE monomer in the EmrE-EmrE $^{\text{E}14\text{Q,L}51\text{I}}$ heterodimer assumes conformation B at pH 5.6. The overlaid spectra in panel (c) are more similar than in panel (d), indicating that the EmrE monomer in the EmrE-EmrE $^{\text{E}14\text{Q,L}51\text{I}}$ heterodimer assumes conformation A at pH 9.5. A few representative peaks are highlighted in red rectangles to underscore the spectral agreement.



Supplemental Figure 6. Distances between the two Glu14 residues in EmrE quantified from molecular dynamics simulations (2).

Histogram of distances between Glu14 residues from molecular dynamics simulations for the proton-bound state of EmrE (E_A^H-E_B^H). Distances were measured from the O^{ε2} atom of Glu14_A to the H^{ε2} atom of Glu14_B.

References

1. K. Schmidt-Rohr, K. J. Fritzsching, S. Y. Liao, M. Hong, Spectral editing of two-dimensional magic-angle-spinning solid-state NMR spectra for protein resonance assignment and structure determination. *J Biomol NMR* **54**, 343-353 (2012).
2. J. V. Vermaas, S. B. Rempe, E. Tajkhorshid, Electrostatic lock in the transport cycle of the multidrug resistance transporter EmrE. *Proc Natl Acad Sci U S A* **115**, E7502-E7511 (2018).